# Nanoscale Advances



## **PAPER**

View Article Online
View Journal | View Issue



Cite this: Nanoscale Adv., 2025, 7, 2068

# Biological and mechanical properties of a selfcuring acrylic resin enriched with AgNPs as a proposal for orthopedic aparatology

Christian Andrea Lopez-Ayuso, Da Rene Garcia-Contreras, Da Ravichandran Manisekaran, Da Mario Figueroa, Db Manuel Rangel-Grimaldo, Dc Mariano Jacome, Ruben Abraham Dominguez-Perez, Dd Salvador Lopez-Morales, Sol Cristians Df and Laura Susana Acosta-Torres D\*\*

Polymethylmethacrylate (PMMA) is widely used in dentistry, but its inherent characteristics, such as roughness and porosity, can facilitate the formation of bacterial biofilms. However, the integration of silver nanoparticles (AgNPs) can provide antimicrobial properties. Ongoing research endeavors aim to preserve post-nanoaggregation biocompatibility without compromising the mechanical integrity of the material. In this study, we investigated the biological and mechanical attributes of a PMMA nanocomposite infused with AgNPs biosynthesized from *Pelargonium* × *hortorum*. A method has been described to incorporate nanoparticles into the polymer at minimum concentrations. In the results, LC-MS-MS revealed the presence of 56 biochemical compounds. UPLCHRESIMS-MS/MS was used to compare the phytochemical profiles of the leaf extract of *Pelargonium* × *hortorum* before and after the formation of AgNPs, which were identified with spherical morphology, an absorbance of 28.5  $\pm$  8.16 nm and a particle size of 415 nm. The MIC of AgNPs was 10  $\mu$ g mL $^{-1}$ . In bacterial MTT, a decrease to 18.2  $\pm$  2.5% with PMMA-10  $\mu$ g mL $^{-1}$  was observed (p < 0.05). Decreased cell viability was found only in PMMA-0  $\mu$ g mL $^{-1}$  at 89.1  $\pm$  6.7%, indicating no cytotoxicity. These findings suggest a promising bionano material that is suitable for orthodontic and orthopedic devices and warrants further research.

Received 12th October 2024 Accepted 1st February 2025

DOI: 10.1039/d4na00846d

rsc.li/nanoscale-advances

## Introduction

Poly[1-(1-(methoxycarbonyl)-1-methylethylene])], is a polymeric material that is synthesized by the addition of free radicals to form polymethyl methacrylate  $[C_5O_2H_8]$  (PMMA);<sup>1,2</sup> its physical, mechanical, optical, low density and thermoplastic properties<sup>2,3</sup> make it biocompatible with the cells of the human body, making it suitable for dental use;<sup>3</sup> the applications in dentistry include dental prostheses,<sup>4</sup> provisional prosthetic restorations<sup>5</sup> and orthodontic appliances to treat malocclusions.<sup>6,7</sup> According to the World Health Organization (WHO), dental malocclusions

Maintaining balance in the oral ecosystem is necessary to promote a healthy state. <sup>16</sup> Still, when this balance is disrupted, dysbiosis occurs, allowing bacteria to manifest and cause diseases such as caries, gingivitis, and periodontitis. <sup>17,19</sup> Due to these problems in clinical practice, in recent years, nanotechnology has shown advances in the development of biomaterials, giving rise to new bioproducts with antimicrobial, antifungal, and tissue regeneration properties, among others. <sup>3,20–22</sup>

To improve the properties of PMMA, it is necessary to incorporate different nanoparticles (NPs), such as zirconium

are considered the third most common oral health problem after caries and periodontal disease, <sup>8,9</sup> with a prevalence of up to 80% in the primary dentition and 70% in the mixed dentition. <sup>10</sup> To correct these alterations, orthopedic devices made of self-curing PMMA are used. <sup>11</sup> However, due to the characteristics of its surface, such as porosity and roughness, <sup>12-14</sup> bacterial colonization can quickly proliferate and cause an increase in volume and concentration of biofilms in this polymer, with an increase in species such as *Streptococcus mutans* and *S. sobrinus*, *Actinomyces* spp., *Pseudomonas* spp., *Lactobacillus* spp., and *Candida albicans*. <sup>15-18</sup> This highlights the critical problem of PMMA's susceptibility to bacterial biofilm formation, necessitating improvements in its antimicrobial properties.

<sup>&</sup>quot;Laboratorio de Investigación Interdisciplinaria, Área de Nanostructuras y Biomateriales, Escuela Nacional de Estudios Superiores Unidad León, Universidad Nacional Autónoma de México (UNAM), Predio el Saucillo y el Potrero, Comunidad de los Tepetates, León, 37684, Mexico. E-mail: lacosta@enes.unam.mx

<sup>&</sup>lt;sup>b</sup>Facultad de Química, UNAM, Ciudad de México, 04510, Mexico

<sup>&#</sup>x27;Instituto de Química, UNAM, Ciudad de México, 04510, Mexico

<sup>&</sup>lt;sup>a</sup>Laboratorio de Investigación Odontológica Multidisciplinaria, Universidad Autónoma de Ouerétaro, Ouerétaro, 76010, Mexico

<sup>&</sup>lt;sup>e</sup>Instituto de Investigaciones en Materiales, Departamento de Reología y Mecánica de Materiales, UNAM, Ciudad de México, 04510, Mexico

<sup>&</sup>lt;sup>f</sup>Laboratorio de Etnobotánica, Instituto de Biología, UNAM, Ciudad de México, 04510, Mexico

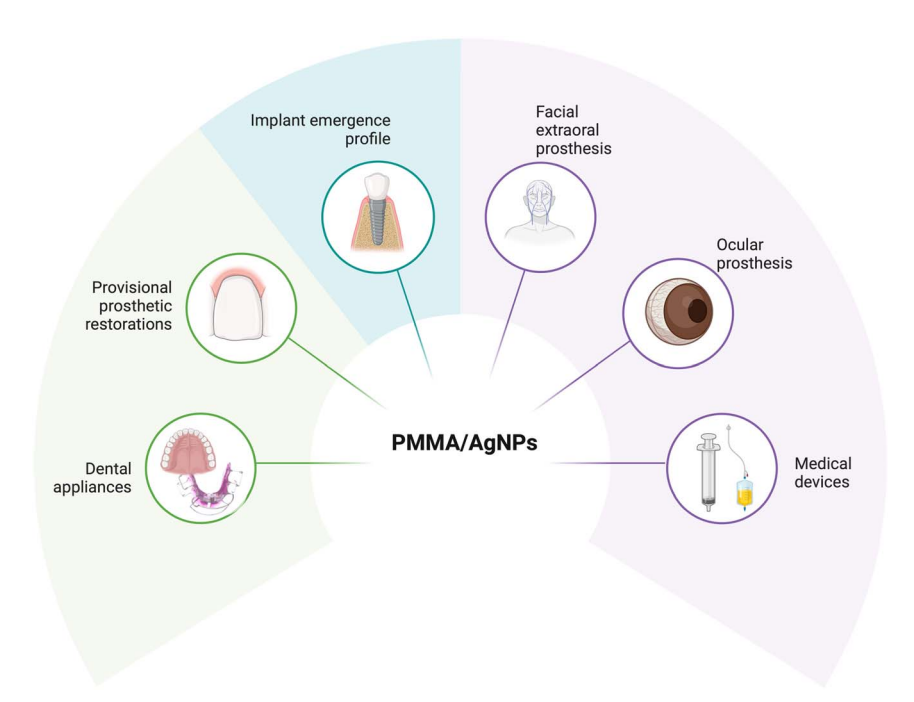


Fig. 1 Potential clinical applications for PMMA composites with AgNPs providing antimicrobial properties and biocompatibility (created in BioRender).

dioxide (ZrO<sub>2</sub>),6 zinc oxide (ZnO),23 titanium dioxide (TiO<sub>2</sub>),24,25 silicon oxide (SiO<sub>2</sub>),<sup>26</sup> aluminum and titanium (Al<sub>2</sub>O<sub>3</sub>/TiO<sub>2</sub>),<sup>27</sup> resveratrol (RNPs),28 and silver nanoparticles (AgNPs).29-31 These new nanometric materials have contributed to advances in nanomedicine and biomedical sciences because of their excellent physical and chemical properties. Among these, AgNPs stand out for their antimicrobial effects, making them a promising addition to PMMA formulations. 22,29-31 However, factors such as filler concentration, particle size, and the type of PMMA (heat-curing or self-curing) must be considered to maintain the biocompatibility and physical and mechanical properties of PMMA with NPs and consequently its biomedical characteristics. This emphasizes the gap in understanding the antimicrobial mechanisms and biocompatibility of PMMA-AgNPs, which this study aims to address.

Therefore, additional investigations are essential to elucidate the antimicrobial mechanisms and biocompatibility profiles of these materials, as well as their potential clinical utility. Consequently, this study aimed to evaluate the biological response encompassing antibiofilm activity against S. mutans, cytotoxicity, oxidative stress, genotoxicity, and proinflammatory responses in HGFs. It also assessed the chemical and mechanical properties, including flexural strength, flexural modulus, and residual monomer content, of self-curing PMMA and PMMA-AgNPs. This innovative formulation proposes a novel approach for orthodontic appliances, addressing the limitations of conventional PMMA materials, that warrants further exploration and validation. Therefore, additional investigations are imperative to elucidate the antimicrobial mechanisms and biocompatibility profiles of these materials, as well as their potential clinical utility (Fig. 1).

## Materials and methods

#### Pelargonium × hortorum extract

An aqueous extract of *Pelargonium*  $\times$  *hortorum* was prepared; the specimen was taxonomically identified prior to the experiment, and a sample was deposited in the Herbarium of the Faculty of Sciences with voucher no. 182314. To obtain the extract, 12.15 g of fresh leaves were cut and added to 100 mL of deionized water (DI water) at boiling point; the extract was maintained at a constant temperature between 90 and 92 °C for 15 min, and then the solution was filtered using a 4-12 µm Whatman filter, to obtain a residue-free extract.

#### **Biosynthesis of AgNPs**

The biosynthesis of AgNPs was carried out using 20 mL of ethylene glycol as a solvent, 10 mL of Pelargonium × hortorum extract as a reducing and stabilizing agent and 1.2 mL of 25 mM silver nitrate (AgNO<sub>3</sub>) (purity ≥ 99%) (Sigma-Aldrich® St Louis, Missouri, USA) as a precursor, added in 0.2 mL increments every 2 min. The solvent, reducing/stabilizing agent and precursor were added in the listed order, and the synthesis was maintained at a constant temperature of 110 °C using a recirculator for 30 min, as reported and detailed in previous experiments.32 The resulting AgNPs were washed twice with 100% acetone (1:4 ratio) and once with absolute ethyl alcohol (1:1 ratio), sonicated for 15 min between each wash, followed by a 15 min centrifugation cycle at 4000 rpm and finally resuspended in deionized (DI) water. The final product was stored at 4 °C for further experiments.

Nanoscale Advances

#### Metabolomic analysis of Pelargonium × hortorum leaves extracts

The leaf extracts of Pelargonium × hortorum before and after AgNP formation were analyzed according to our previous work32 using an ultra-performance liquid chromatographic system (UPLC; Acquity, Waters Corp., Milford, MA, USA) coupled with a high-resolution mass spectrometer tandem MS/MS (HRESIMS-MS/MS; Q-Exactive Plus, Thermo Fisher Scientific, Waltham, MA, USA) equipped with an electrospray source (ESI) in positive and negative modes. The molecular networks were created using the GNPS (https://www.gnps.ucsd.edu) platform, using the same parameters as in our previous work.<sup>32</sup> Finally, the MS data were subjected to principal component analysis (PCA) using the online platform MetaboAnalyst 5.0.33

## Preparation of self-curing acrylic resin compounds with **AgNPs**

Samples of self-curing PMMA NicTone (MDC Dental® Gardena, CA, USA) and Opti-Cryl (New Stetic, S.A. CDMX, Mexico), clear color, were prepared with 0, 5, 10, 15 and 20  $\mu g$  mL<sup>-1</sup> of AgNPs. The methodology was as follows: the concentration of AgNPs was calculated and they were placed in 1.5 mL Eppendorf tubes; the volume of all groups was adjusted to 0.5 mL with DI water and centrifuged at 13 000 rpm for 10 min; the supernatant was removed and the pellet containing the AgNPs was retained; then 1 mL of monomer corresponding to each of the brands used was added and sonicated for 15 min to allow the dispersion of the NPs into the monomer; then a mixture of the monomer and polymer was made following the manufacturer's instructions in a 3:1 ratio (powder-liquid). The compounds were obtained by pressing this mixture in stainless-steel molds of 10 mm diameter and 2 mm thickness until polymerization was achieved (Fig. 1). Once the samples were obtained, they were polished to eliminate irregular edges. Finally, they were subjected to a sterilization cycle at 121 °C for 15 min and stored for biological experiments.

#### Characterization techniques

The optical properties of the AgNPs were analyzed with UV-visible spectroscopy (Multiskan Go, Thermo Fisher Scientific™, Finland) in the wavelength range of 300-600 nm with a resolution of 1 nm. The morphology was analyzed using transmission electron microscopy (TEM, JEOL, JEM-1010 Tokyo, Japan) at an accelerating voltage of 80 kV. The size distribution was estimated based on the TEM micrograph using ImageJ software (NIH, Maryland, USA). To confirm the crystalline nature of AgNPs, an X-ray diffraction (XRD) analysis (Bruker XDR, 2D Phaser, Billerica, Massachusetts, USA) with Cu-Kα radiation (1.54 Å), was carried out. To verify the presence of AgNPs in the monomer, an analysis was performed by inductively coupled plasma source mass spectrometry (ICP-MS, iCAP QR, Thermo Scientific, Waltham, Massachusetts, USA). Prior to sample analysis, the instrument was optimized using a certified aqueous solution of high-purity standards (Li, Co, In, Ba, Bi, Ce, and U at 1 µg L<sup>-1</sup>). For metal analysis, a 10-point calibration curve (0, 1, 1, 2.5, 5, 7.5, 10, 25, 50,

50, 75, and 100  $\mu$ g L<sup>-1</sup>) was established from single-element solutions of Ag at 1000 μg mL<sup>-1</sup>. Instrumental drift was corrected using the internal standard rhodium (Rh at 10  $\mu$ g L<sup>-1</sup>). The limits of detection were calculated using the following equation L. D. = 3(SD int BCO)(conc. STD)/(int STD - prom int)BCO), where SD int BCO - standard deviation of the blank intensity; conc. STD - concentration of the standard solution; int STD - intensity of the standard solution and prom int BCO average of the blank intensity.

#### **Biological response studies**

Microbial culture. Culture media were obtained from Mueller Hinton Agar (Sigma-Aldrich® St Louis, Missouri, USA); Petri plates were inoculated with S. mutans (ATCC-35668), and incubated at 37 °C for 24 h. Overnight cultures were obtained by transferring 10 colonies from these plates to Brain and Heart Infusion (BHI) medium (Sigma-Aldrich® St Louis, Missouri, USA), followed by incubating at 37 °C for 16-20 h. Bacterial concentrations were measured using a densitometer (Grant Instruments™ DEN-1B, Cambridgeshire, UK). The bacterial inoculum was calculated using standard turbid solutions (McFarland scale, 0.5). This opacity is equivalent to  $1 \times 10^8$  CFU mL<sup>-1</sup>. The bacterial MTT assay<sup>34,35</sup> was used to determine biofilm formation in the self-cured PMMA composites with and without AgNPs.

Biofilm formation. The bacterial inoculum was diluted to obtain  $1 \times 10^5$  CFU mL<sup>-1</sup> of bacterial suspension in BHI supplemented with 0.6% sucrose as a growth medium. Self-curing PMMA composites with 0 (control), 5, 10, 15, and 20  $\mu g \text{ mL}^{-1}$ AgNPs were added to 24-well plates. The plate was incubated in a shaking incubator at 37 °C and 180 rpm for 5 days, and the medium was changed every 24 h. Samples were then transferred to new plates and washed three times with sterile phosphatebuffered saline (PBS) to remove the unattached biofilm. Then, a 3-(4,5-dimethylthiazol-2-yl)-2,5-diphenyltetrazolium bromide (MTT) standard was prepared at  $2 \text{ mg mL}^{-1}$  in fresh BHI culture medium, and the plates were sonicated at 37 kHz with 50% power for 5 min to promote biofilm detachment from the samples, followed by incubation at 37 °C for 2 h. Formazan crystals were dissolved in 0.5 mL of dimethyl sulfoxide (DMSO, Karal, Guanajuato, Mexico) and transferred to a 96-well plate for analysis using a Multiskan GOTM at 550 nm. The experiments were repeated in triplicate from three independent experiments (n = 9 for each concentration), and the results are expressed as the average percentage of microbial adherence compared with the control (Fig. 2).

Scanning electron microscopy (SEM). Three disks from the NicTone and Opti-Cryl experimental groups with 0 and 10  $\mu g$ mL<sup>-1</sup> AgNPs were analyzed using SEM (Joel-JSM-6360 OLV. Tokyo, Japan). After 5 days of biofilm formation (BHI supplemented with and without 0.6% sucrose), the samples were gently washed three times with PBS to remove non-adherent cells. The samples were fixed in ethanol with 10% formol for 10 min, then washed three times with DI water, dried and placed on gold sputter-coated copper supports and observed at 6500× magnification (Fig. 2).

Paper

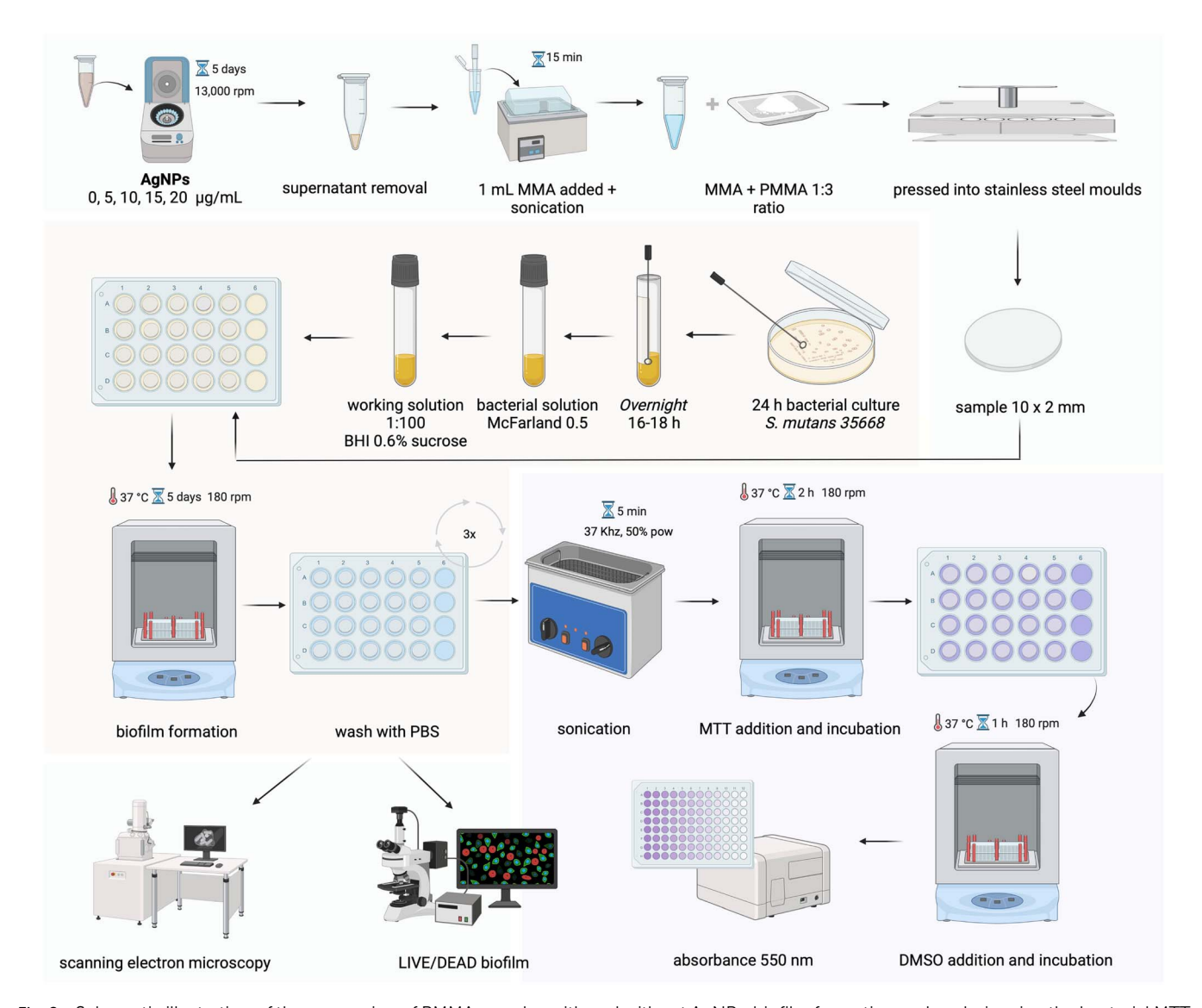


Fig. 2 Schematic illustration of the processing of PMMA samples with and without AgNPs, biofilm formation and analysis using the bacterial MTT assay, scanning electron microscopy (SEM) and confocal microscopy for the LIVE/DEAD™ reagent (created in BioRender).

LIVE/DEAD biofilms. The fluorescence from live and dead stained cells adhered to NicTone and Opti-Cryl test samples with 0 and 10  $\mu g \text{ mL}^{-1} \text{ AgNPs} (n = 3)$  was observed using a confocal microscope (LSM 780) after 5 days of biofilm formation (BHI supplemented with 0.6% sucrose). The fluorescent marker LIVE/DEADTM reagent (BaclightTM Invitrogen Thermo Fisher Scientific™, Massachusetts, USA) was prepared by mixing 1  $\mu$ L of Syto 9 and 1  $\mu$ L of propidium iodide (PI) in 1 mL of sterile water. Subsequently, the samples were gently washed three times with PBS to remove non adherent cells; then 100  $\mu L$  of LIVE/DEAD<sup>TM</sup> reagent was added to each sample and left to act for 3 min. Then, ten randomly selected image sections were recorded for each biofilm sample. Confocal images were obtained using a 40× objective and digitized using Leica Application Suite Advanced Fluorescence Software at  $512 \times 512$ pixels, with a  $1\mu$  interlayer for optical imaging (Fig. 2).

Cell culture assays. HGFs were obtained from a gingival tissue biopsy during third molar surgery from a 21-year-old

patient who previously signed an informed consent form, as described in previous studies.32 The protocol was endorsed by the internal Bioethics Committee of the ENES, Campus Leon, with registration number CE\_16/004\_SN. HGFs were inoculated at a ratio of 1:3 into 96-microwell plates and incubated for 24 h in fresh Eagle's Minimum Essential Medium (MEM) culture medium, supplemented with 10% sterile fetal bovine serum (FBS), 1% antibiotics (10 000 IU mL<sup>-1</sup> penicillin G and 10 000 mg mL<sup>-1</sup> streptomycin, Sigma-Aldrich, Mexico), and 1% glutamine (Glutamax, Gibco® Thermo Fisher Scientific™, Massachusetts, USA). Petri dishes were incubated at 37 °C with 5% CO<sub>2</sub> and 95% relative humidity (Thermo Fisher Scientific™) to allow fixation for cell-based studies.

Cytotoxicity test. The cytotoxic effect of NicTone and Opti-Cryl samples with 0 and 10  $\mu g\ mL^{-1}$  AgNPs was evaluated using HGF  $1 \times 10^6$  cells per mL, grown in 24-microwell plates for direct contact analysis and in 96-microwell plates for indirect contact. The incubation was maintained at 37 °C, 5% CO<sub>2</sub>,

and 95% relative humidity for 24 h. For direct contact, discs with 0 and 10 µg mL<sup>-1</sup> AgNPs were placed floating on the culture medium. For indirect contact, 1 sample was placed in 1 mL of sterile MEM before experimentation and stirred at 180 rpm, 37 °C for 24 h. After this, the disc was removed, and the resulting elution was added to the corresponding 96-well plates. After 24 h of exposure, the standard 3-(4,5dimethylthiazol-2-yl)-2,5-diphenyltetrazolium bromide (MTT) method was used determine the viable cell number using 2 mg mL<sup>-1</sup> MTT in fresh culture medium. The formed formazan was dissolved in 0.1 mL of dimethyl sulfoxide (DMSO, Karal, Guanajuato, Mexico) for 96-microwell plates and in 0.3 mL for 24microwell plates, and absorbance readings were taken on a Multiskan GO™ at 570 nm. The experiments were performed in triplicate from three independent experiments (n = 9), and the results were expressed as an average percentage of viable cell numbers and compared with the control (untreated).

Oxidative stress assay. Reactive oxygen species (ROS) analysis was performed with an intracellular ROS fluorometric assay kit (Sigma-Aldrich®) using HGF at a cell density of  $1\times 10^5$  cells per mL when exposed to NicTone and Opti-Cryl with 0 and 10 µg mL<sup>-1</sup> AgNPs (direct and indirect contact); a hydrogen peroxide concentration (H<sub>2</sub>O<sub>2</sub>) of 2 mM was used as a positive control and sterile culture medium (MEM) was used as a negative control. The experiment was performed for 24 h, and subsequently, the ROS detection reagent was freshly prepared by dispersing it in 40 µL of DMSO. Finally, 100 µL of fresh reagent was added to each well and incubated for 1 h (37 °C, 5% CO<sub>2</sub>, 95% relative humidity), and fluorescence was measured at  $\lambda_{\rm ex} = 490$  nm/ $\lambda_{\rm em} = 520$  nm using a GO<sup>TM</sup> Multiskan reader.

Genotoxicity assay. The indirect contact of NicTone and Opti-Cryl with 0 and 10 μg mL<sup>-1</sup> AgNPs was studied using HGF cell culture at a cell density equivalent of  $1 \times 10^6$  cells. Cells were cultured on sterile glass in 24-well plates in supplemented MEM culture medium for 24 h (37 °C, 5% CO<sub>2</sub>, 95% relative humidity). The positive control was 2 mM H<sub>2</sub>O<sub>2</sub> and the negative control was sterile culture medium. Incubation with test samples was carried out for 24 h. Qualitative analysis of cell nuclei was then performed using a DAPI (4',6-diamidino-2phenylindole, Sigma-Aldrich® St Louis, Missouri, USA) fluorescence assay. Briefly, the samples were washed twice with PBS, fixed with 2% glutaraldehyde (Sigma-Aldrich® St Louis, Missouri, USA) for 10 min, washed once with PBS, and finally DAPI solution (0.5 μL in 1 mL PBS) was added. The samples were kept in the dark without incubation and analyzed directly using a super-resolution microscope - ELYRA - ZEISS at  $63 \times$ magnification.

**Proinflammatory response.** A western blotting assay was performed to determine the proinflammatory response of COX-1 and COX-2. As a positive control, cultures were induced into a proinflammatory state using 12 ng mL $^{-1}$  human interleukin 1-β (IL-1β human recombinant, R&D Systems, Minneapolis, MN, USA) for 3 h; sterile MEM was used as the negative control; then the direct and indirect contact of NicTone with 0 and 10 μg mL $^{-1}$  AgNPs was carried out for 24 h. Protein lysis and extraction were performed with 1× RIPA lysis buffer (Biotechnology WVR AMRESCO, Fountain Parkway, Solon, OH, USA) which was

kept for 15 min on ice at 4 °C; then the cells were scrapped with a spatula and the lysed culture was sonicated for 15 s and centrifuged at 12 000 rpm for 10 min at 4 °C. A protease inhibitor cocktail (cOmplete Roche Diagnostics, Indianapolis, IN, USA) was added. The concentration of proteins in the lysates was determined by the Bradford method; then 30 µg mL<sup>-1</sup> of proteins were loaded for 12% SDS-polyacrylamide gel electrophoresis (SDS-PAGE), and the proteins were transferred to a membrane of polyvinylidene fluoride (PVDF, immobilon®-P Transfer Membranes, Sigma-Aldrich® St Louis, Missouri, USA). Blocking was performed with a 3% nonfat milk solution for 2 h at room temperature (RT) and anti-COX-1, anti-COX-2 and βactin monoclonal antibodies were incubated (Santa Cruz Biotechnology, Dalla, TX, USA) at a dilution of 1:1000 in 3% blocking solution for 1 h 45 min, followed by four 5 min washes with 0.05% phosphate buffer saline with Tween detergent (PBST); then horseradish peroxidase-coupled polyclonal antimouse IgG antibodies were diluted (Sigma-Aldrich® St Louis, Missouri, USA) 1:10 000 in 3% blocking solution and incubated for 1 h at room temperature. The formed complexes were visualized by chemiluminescence using the Cytiva Lifescience™ western Blot Detection Reagent (Amersham™ ECL™ Prime, Marlborough, USA) and the results were visualized using the C-Digit Blot Scanner (Li-Cor, Lincoln, NE, USA) and the density of the bands was analyzed using Software Image J (NIH, Maryland, USA).

Residual monomer. Three samples of NicTone and Opti-Cryl with 0 and 10  $\mu g \text{ mL}^{-1}$  AgNPs, each with a diameter of 50 mm and a depth of 3.0  $\pm$  0.1 mm were made for solvent extraction of the methyl methacrylate monomer (MMA) in accordance with ISO 20795-2:2013.36,37 For the test, each sample was fragmented and the mass of the sample was placed in a volumetric flask into which 10 mL of tetrahydrofuran (THF) solvent was added and the mixture was stirred for 72  $\pm$  2 h at room temperature. To quantify the residual monomer and to precipitate the dissolved polymer, a 2 mL aliquot of the sample solution was transferred to a 10 mL volumetric flask and 100 µL of internal standard (decane) was added; methanol was added to a total volume of 10 mL and allowed to stand for 24 h (until a clear solution was observed). Quantification and analysis were performed using a gas chromatograph with a flame ionization detector (GC-FID, GC-2010, Shimadzu® Restek® USA). Each sample was injected in triplicate.37

Mechanical properties. Ten samples  $(64 \pm 1 \text{ mm long}, 10.0 \pm 0.2 \text{ mm wide}, \text{ and } 3.3 \pm 0.2 \text{ mm in height})$  of NicTone and Opti-Cryl with 0 and 10  $\mu\text{g mL}^{-1}$  AgNPs were prepared. They were kept in deionized water at 37  $\pm$  1 °C for 50  $\pm$  2 h before mechanical testing. The three-point test was carried out; each sample was mounted with its edges equidistant from the midline of the base supports separated by 50 mm. The load was applied at a crosshead speed of 5 mm min<sup>-1</sup> until each sample fractured. Data were collected in Newtons and then converted to megapascals (MPa) using the following equation: flexural strength = 3Fl/(2bh2), where [F] represents the maximum load, [I] is the distance between supports (mm), [b] is the width of the specimen (mm), and [h] is the height (mm). The flexural modulus was determined in gigapascals (GPa) using the

Paper Nanoscale Advances

equation  $E = F_1 l^3 / 4bh^3 d$ , where  $[F_1]$  represents the maximum load (N), [l] is the distance between supports (mm), [b] is the width of the test tube (mm), [h] is the height (mm), and [d] is the deflection (mm) corresponding to the load F as described in ISO 20795-2:2013.36

#### Statistical analysis

Data obtained from all the experiments are expressed as mean and  $\pm$  standard deviation of at least three independent experiments. Data analysis was performed using IBM® SPSS Statistics 29.0 and distribution was assessed using Shapiro-Wilk, ANOVA and Tukey's post hoc test, and p < 0.05 values were statistically significant.

## Results and discussion

#### Biosynthesis and characterization of AgNPs

The color change, from light green to amber, during the formation of AgNPs by green synthesis with Pelargonium × hortorum extract is shown, along with the surface plasmon resonance absorption at 412 nm in the UV-vis spectrum (Fig. 3A); this is typical of AgNP formation as reported in previous studies,32 and is consistent with findings from other researchers who suggest that the identification of high absorptions peaks in the spectrum between 400 and 450 nm is related to the formation of silver nanoclusters.38-40 Spherical spectra are related to a single band, while particles of different morphologies can give rise to two or more bands;41 so, our results from a single absorption band are consistent with this morphology, as shown in Fig. 3B, where the transmission electron microscope image reveals monodisperse nanoparticles of hemispherical morphology with an average size of 27.9  $\pm$ 9.2 nm. In Fig. 3C, the diffraction patterns of AgNPs are depicted, revealing diffraction peaks indicative of the presence of Ag<sup>0</sup>. Specifically, the peaks located at  $2\theta$  angles of 38.35°, 44.36°, 64.64°, and 77.65° correspond to the (111), (200), (220), and (311) crystal planes, respectively, according to the JCPDS: 04-0783 crystallographic chart. These peaks confirm the facecentered cubic (FCC) structure of the AgNPs obtained in this

study, thus validating the presence of elemental silver, in line with the findings reported by other researchers. 42,43

## Chemical changes in the compositions of *Pelargonium* × hortorum leaf extracts after AgNP formation

Recently, we described the chemical composition of the Pelargonium × hortorum leaf extract using untargeted metabolomic analysis.32 The metabolite features present in the leaf extracts before and after AgNP formation were grouped into 1706 nodes arranged in 79 clusters with >3 nodes per cluster, 82 with two nodes, and 802 singletons (Fig. 4). From the total number of nodes, 412 were observed only in the extract after AgNP formation, while 691 were exclusive to the original extract before treatment. This indicates that the reaction during the formation of AgNPs affected the chemical composition of the extract.

Principal component analysis (PCA) of the metabolite features observed by LCMS analysis clearly differentiated the Pelargonium × hortorum leaf extracts before and after treatment (PC1 = 97.8% versus PC2 = 1.1%; Fig. 5). The metabolites identified by GNPS for each treatment are shown in Table 1 and Fig. 6. Interestingly, the 24 metabolites identified in our previous work32 were not found in the leaf extract after AgNP formation. In addition, 24 metabolites were shared between the extracts from the 29 metabolites observed in the extract before AgNP formation. The major components of the plant extract were flavonoids and its glycosides, followed by O-glycosyl and phenylpropanoid compounds (tannins), and cyclitol derivatives (Fig. 6).

#### Self-curing acrylic resin compounds enriched with AgNPs

PMMA is a long polymer obtained through a chemical polymerization process in which the monomers react in steps between two molecular species (R and R'), which must contain at least two functional groups. When these compounds react, they join to form chains or networks of three-dimensional particles.44 The PMMA synthesis involves the addition of 0, 5, 10, 15, and 20  $\mu$ L mL<sup>-1</sup> of AgNPs to NicTone and Opti-Cryl monomers. Subsequently, the polymer-monomer mixture was

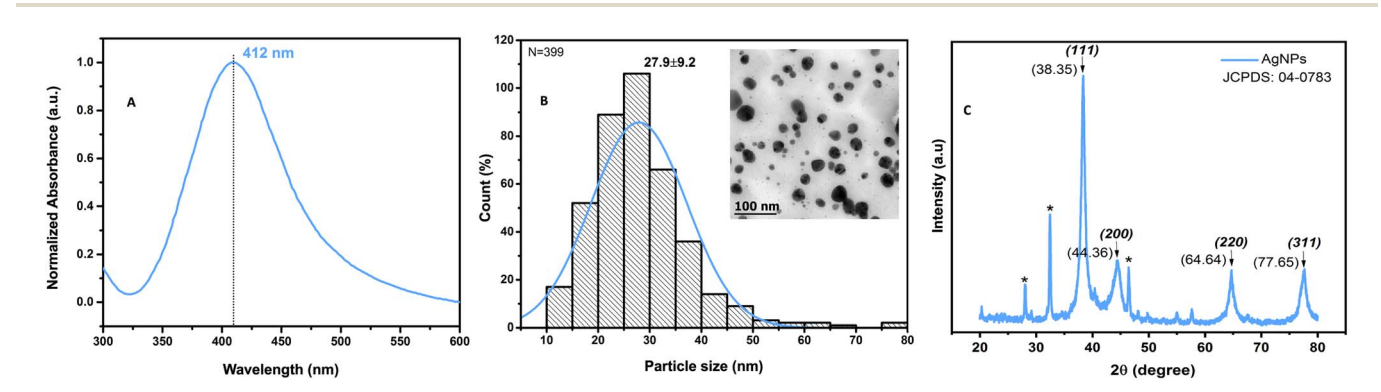


Fig. 3 UV-vis spectrum, TEM micrograph, and XRD pattern of AgNPs. Absorption spectra of AgNPs obtained from Pelargonium × hortorum at 412 nm (A), the TEM micrograph taken at a magnification of 100k× and 80 kV showing monodisperse nanoparticles with a mean particle size of  $27.9 \pm 9.2$  nm and hemispherical morphology (B), and the different diffraction peaks corresponding to the lattice plane values of silver crystals according to the standard (JCPDS) file no. 04-0783 (C).

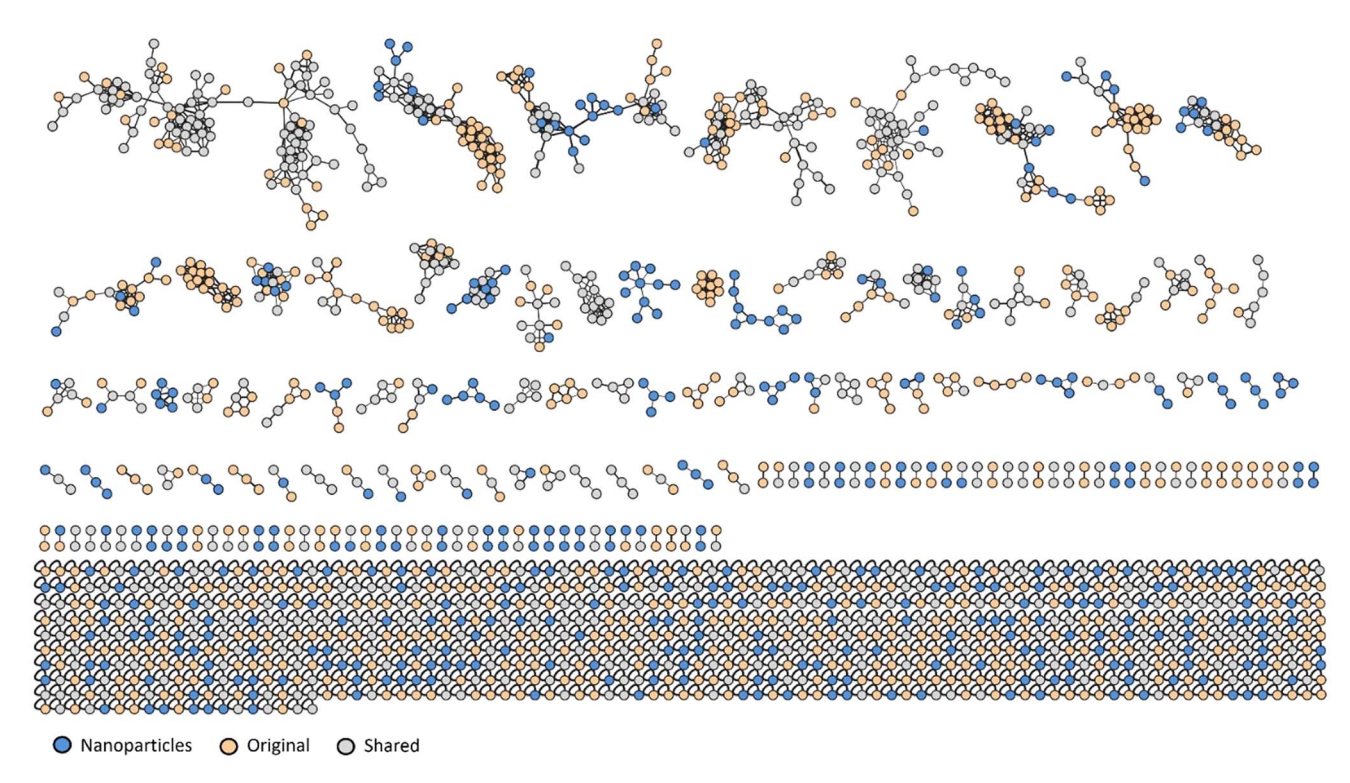


Fig. 4 Molecular networking of Pelargonium × hortorum leaf extracts before and after AgNP formation.

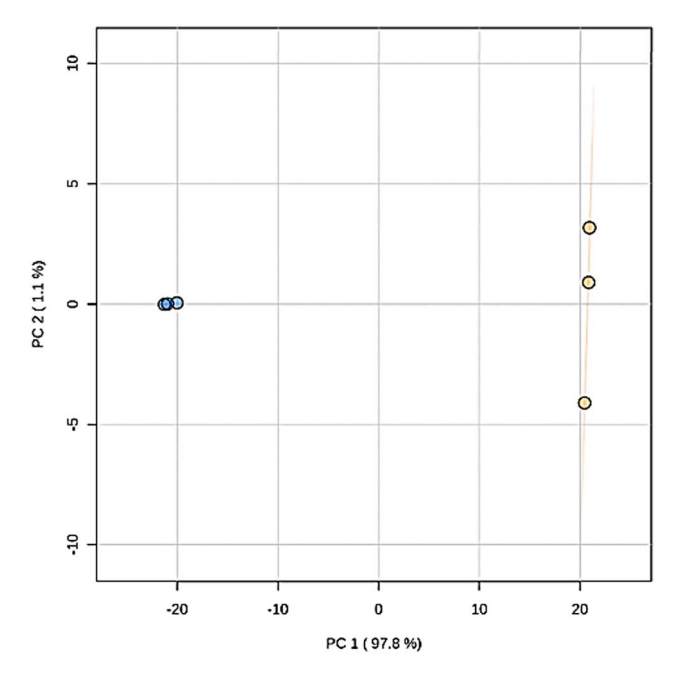


Fig. 5 Nanoparticle treatment effect on the overall metabolomic profile determined by PCA of *Pelargonium* samples. Orange, original extract; blue, nanoparticle treatment. The PCA score plot derived from positive (ESI $^+$ ) and negative (ESI $^-$ ) modes in LC-MS metabolite profiles of *Pelargonium*  $\times$  *hortorum* leaf extracts before and after AgNP formation.

prepared in a 3:1 ratio to initiate the polymerization reaction, following the methodology previously reported by Acosta-Torres *et al.*;<sup>22</sup> the ICP-MS results indicated the presence of 15.623 ppm

Ag in the monomer. Campos *et al.* reported the coating of AgNPs on Opti-Cryl using a sprayed solution with a concentration of 338 ppm; the authors analyzed the release of silver in an aqueous medium considering that the addition was by impregnation on the surface, identifying a release of 0.48 ppm after eight days of experimentation achieving antimicrobial activity. According to Flores-Arriaga *et al.*, low concentrations of AgNPs at the filler level in the polymer interfere with the formation of bacterial biofilms through an anti-adherent effect. In the polymer interfere with the formation of bacterial biofilms through an anti-adherent effect.

#### **Biofilm formation**

The adherence of S. mutans biofilms to PMMA and PMMA/AgNP composites was analyzed using the bacterial MTT assay.34,35 Fig. 7 shows 91.6  $\pm$  4.7% adherence of *S. mutans* biofilms on PMMA from the NicTone brand without the incorporation of AgNPs (0  $\mu g \; mL^{-1}$ ), which decreased to 18.2  $\pm$  2.8% with 10  $\mu g$  $mL^{-1}$  AgNPs (p < 0.05). The Opti-Cryl brand presented an adherence of 49.5  $\pm$  3.3%, decreasing to 16.7  $\pm$  2.4% with 15  $\mu g$  ${\rm mL}^{-1}$  (p < 0.05). The AgNPs biosynthesized in this study showed antimicrobial activity against S. mutans at 10  $\mu$ g mL<sup>-1</sup>, <sup>32</sup> as described previously. These results are consistent with those of with Tavaf et al., who also reported a minimum inhibitory concentration at 10 µg mL<sup>-1</sup>, and are close to the ranges reported by Ma et al., at 8.5 μg mL<sup>-1</sup>.46,47 Campos et al.45 reported antimicrobial effects on Escherichia coli (6.74 µg mL<sup>-1</sup>) and Staphylococcus aureus (13.48 µg mL<sup>-1</sup>) in PMMA with AgNP compounds. These results, despite having been analyzed in other bacteria, are similar to our results, where a decrease in microbial adherence was found at 5, 10, and 15  $\mu g$  mL<sup>-1</sup> AgNPs.

Table 1 GNPS chemical annotation of metabolites in *Pelargonium* × hortorum leaf extracts before and after AgNP formation

Compounds	Observed ion <sup><math>a</math></sup> ( $m/z$ )	Adduct	Molecular formula [adduct]	Exact mass (calculated)	Mass accuracy (ppm)
Galactaric acid <sup>c</sup>	209.030	[M – H] <sup>-</sup>	$C_6H_9O_8$	209.0303	-1.4
Pantothenic acid <sup>b</sup>	220.118	$[M + H]^{+}$	$C_9H_{18}NO_5$	220.1179	+0.2
Malic acid <sup>b</sup>	289.018	[2M + Na – 2H]	$C_8H_{10}O_{10}Na$	289.0177	+1.0
2-Phenylethyl β-D-glucopyranoside <sup>c</sup>	302.161	$[M + NH_4]^+$	$C_{14}H_{24}NO_6$	302.1598	+3.9
2-Coumaroylquinic acid <sup>c</sup>	339.109	$[M + H]^{+}$	$C_{16}H_{19}O_{8}$	339.1074	+4.6
Coumaric acid 4- <i>O</i> -glucoside <sup>c</sup>	344.135	$[M + NH_4]^+$	$C_{15}H_{22}NO_8$	344.1340	+2.9
Chlorogenic acid <sup>c</sup>	353.088	$[M-H]^{-1}$	$C_{16}H_{17}O_{9}$	353.0878	+0.6
Coumaroyl + $C_6H_9O_8^c$	355.068	$[M - H]^-$	$C_{15}H_{15}O_{10}$	355.0671	+2.6
3-O-Feruloylquinic acid <sup>c</sup>	367.104	$[M - H]^-$	$C_{17}H_{19}O_{9}$	367.1034	+1.5
NP-006680: 3-(benzoyloxy)-2-	371.099	$[M - H]^-$	$C_{16}H_{19}O_{10}$	371.0984	+1.7
hydroxypropyl $\beta$ -D-glucopyranosiduronic acid $^c$		. ,	10 13 10		
NP-016360: 3,5,5-trimethyl-4-[3- [(β-p-glucopyranosyl)oxy]butyl]-3- cyclohexen-1-ol <sup>c</sup>	375.239	$[M + H]^+$	$C_{19}H_{35}O_{7}$	375.2377	+3.4
NP-001173: [5-hydroxy-2-(3- hydroxybutyl)-3,3-dimethylcyclohexyl] methyl β-p-glucopyranoside <sup>c</sup>	393.249	$[M + H]^+$	$C_{19}H_{37}O_{8}$	393.2483	+1.8
Kaempferol 3-α-1-arabinopyranoside <sup>c</sup>	417.083	$[M - H]^-$	$C_{20}H_{17}O_{10}$	417.0827	+0.7
Icariside F2 <sup>c</sup>	420.188	$[M + NH_4]^+$	$C_{18}H_{30}NO_{10}$	420.1864	+3.8
Avicularin <sup>c</sup>	435.093	$[M + H]^{+}$	$C_{20}H_{19}O_{11}$	435.0922	+1.9
Luteolin 4'-O-glucoside <sup>b</sup>	447.094	$[M - H]^-$	$C_{21}H_{19}O_{11}$	447.0933	+1.6
Astragalin <sup>c</sup>	449.109	$[M + H]^{+}$	$C_{21}H_{21}O_{11}$	449.1078	+2.6
Isoquercetin <sup>c</sup>	463.089	$[M - H]^-$	$C_{21}H_{19}O_{12}$	463.0882	+1.7
1,6-Digalloyl-β-D-glucopyranose <sup>b</sup>	502.121	$[M + NH_4]^+$	$C_{20}H_{24}NO_{14}$	502.1191	+3.7
Procyanidin B2 <sup>b</sup>	577.136	$[M-H]^{-1}$	$C_{30}H_{25}O_{12}$	577.1352	+1.5
6"-O-(3-Hydroxy-3-methylglutaroyl) astragalin <sup>c</sup>	591.137	$[M-H]^-$	$C_{27}H_{27}O_{15}$	591.1355	+2.5
Nicotiflorin <sup>c</sup>	593.152	$[M - H]^-$	$C_{27}H_{29}O_{15}$	593.1512	+1.4
2"-O-Galloylhyperin <sup>c</sup>	615.101	$[M + H]^+$	C <sub>28</sub> H <sub>23</sub> O <sub>16</sub>	615.0992	+3.0
Mauritianin <sup>c</sup>	739.211	$[M-H]^-$	C <sub>33</sub> H <sub>39</sub> O <sub>19</sub>	739.2091	+2.6
Kaempferol 3-O-(2,6-di-O-alpha-L-	739.210	$[M-H]^-$	$C_{33}H_{39}O_{19}$	739.2091	+1.2
rhamnopyranosyl)-β-D- galactopyranoside <sup>c</sup>		. ,	- 33 39 - 19		
Quercetin 3-(2 <i>R</i> -apiosylrutinoside) <sup>c</sup>	741.190	$[M - H]^-$	$C_{32}H_{37}O_{20}$	741.1884	+2.2
Manghaslin <sup>c</sup>	757.222	$[M + H]^+$	C <sub>33</sub> H <sub>41</sub> O <sub>20</sub>	757.2186	+4.5
1,2,3,6-Tetragalloylglucose <sup>c</sup>	787.102	$[M-H]^-$	$C_{34}H_{27}O_{22}$	787.0999	+2.6
Pentagalloylglucose <sup>c</sup>	939.113	$[M-H]^-$	$C_{41}H_{31}O_{26}$	939.1109	+2.2

<sup>&</sup>lt;sup>a</sup> Values taken from GNPS analysis. <sup>b</sup> Compounds observed in the extract before AgNP formation. <sup>c</sup> Compounds shared in the extracts.

In the present study, the AgNPs were inside the material and were incorporated into the monomer, as described by other researchers. 22,48 Several reports in the literature indicate that the antibacterial and antibiofilm efficacy of AgNP-incorporated materials depends on the release of silver ions and their direct contact with bacteria.38,48

According to the SEM images (Fig. 8), notable differences were observed between the PMMA groups with and without AgNPs. A comparison of biofilm images showed changes in biofilm growth on self-curing PMMA, which was observed to be dispersed in the absence of sucrose. However, these biofilms developed homogeneously with areas of greater structural maturity and more homogeneous growth with a sucrose supplementation of 0.6% in the culture medium, suggesting that its presence favors the growth and structure of biofilms. 49 This significantly higher accumulation of S. mutans is related to

elevated levels of polysaccharides, such as glucans, which are the main constituents of the S. mutans biofilm matrix, providing a three-dimensional scaffold and attachment sites to support this bacterial coaggregation. The reduced biofilm formation on nanoparticle polymers may be due to the inability of bacteria to use these polyols as substrates for the synthesis of biofilm matrices.49,50 Since the SEM images only showed the biofilm volume, a Live/Dead™ BacLight bacterial viability kit was used to evaluate the effect of PMMA and PMMA/AgNP composites. Fig. 8 shows the presence of a higher biovolume of live-cell bacteria (green) in PMMA without the addition of AgNPs. This biofilm showed an increase in dead cells (red) in PMMA with 10  $\mu g \text{ mL}^{-1} \text{ AgNPs}$ , mainly for the NicTone group with 10  $\mu g \text{ mL}^{-1}$ AgNPs and these results correlate with those identified in the MTT assay, showing the presence of a greater biovolume of live bacterial cells.

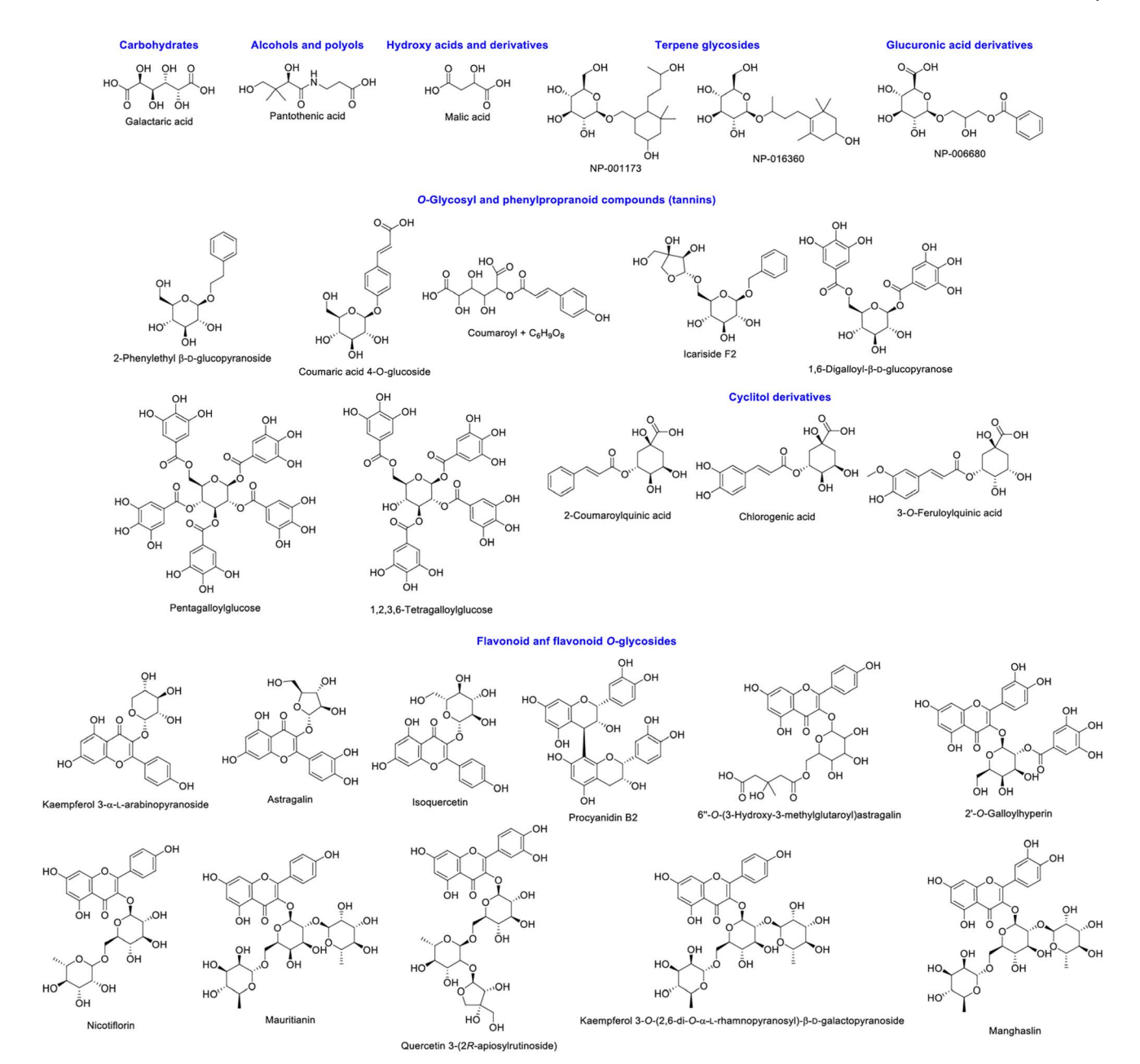


Fig. 6 Structures of the identified compounds in *Pelargonium* imes *hortorum* leaf extracts

#### Cytotoxicity assay

The cytotoxic effect of biosynthesized AgNPs was identified in previous studies with a dose-dependent response, with moderate cytotoxicity, with the mean cytotoxic dose (CC<sub>50</sub>) being found at a concentration of 4.5  $\mu g$  mL $^{-1}$ , as described in previous reports. $^{32}$  For the HGF assays, from the cell viability test, 10  $\mu g$  mL $^{-1}$  AgNPs were incorporated into the PMMA, as this was the concentration at which statistically significant differences were found in both brands analyzed. A decrease in cell viability was observed for the NicTone groups with 0 and 10  $\mu g$  mL $^{-1}$  in direct contact, and for the Opti-Cryl group with 10  $\mu g$  mL $^{-1}$  in indirect contact (p < 0.05); however, the viability percentage in these groups was greater than 80%, which means

that they did not present cytotoxicity.  $^{51}$  Furthermore, in all other groups, a hormesis effect was observed (Fig. 9A). These results are consistent with those of Sun *et al.*, who confirmed the biocompatibility of PMMA with AgNPs at the cellular level using MTT and *in vivo* assays in experiments with rabbits and mice.  $^{52}$  In contrast, Pinheiro *et al.* found greater cytotoxicity in groups with AgNPs incorporated into or immersed in PMMA.  $^{53}$  For this reason, the nanoparticle incorporation technique plays an important role in the cellular response; in our study, the independent analysis of AgNPs showed a 50% decrease in cell viability at  $4.5~\mu g$  mL $^{-132}$  compared to incorporating  $10~\mu g$  mL $^{-1}$  in self-curing PMMA, which maintained it above 80%. When the polymers are immersed in PMMA, the decrease in cell viability is greater in the first 24~h, because AgNPs exhibit high diffusion

Paper

NicTone 100 Opti-Cryl S. mutans biofilm adherence (%) 80 60 40 20 PMMA-AgNPs composites (µg/mL)

Fig. 7 Adherence analysis of S. mutans biofilms to PMMA-AgNP composites on NicTone and Opti-Cryl with 0, 5, 10, 15, and 20 g  $\rm mL^{-1}$ AgNPs was evaluated using bacterial MTT assay. Optical density 550 nm. Abs. range (0.062-0.709), where each value represents the percentage of the mean and S.D. One-way ANOVA, post hoc Tukey; (\*) represents concentrations with significant difference; p < 0.05, n = 9 in independent experiments in triplicate.

in aqueous media;53 however, when incorporated during the polymerization process, the metallic silver is possibly encapsulated in the polymer, reducing the percentage of release into the medium and thus promoting cell viability.54

#### Oxidative stress

The reactive oxygen species (ROS) experiment showed a slight increase in the production of free radicals in the study groups without statistically significant results (p > 0.05) (Fig. 9B). While in the evaluation of nuclear morphology using DAPI and fluorescence microscopy, continuity of the cell nuclei can be observed for the negative control groups (HGF), in the PMMA and self-healing PMMA-AgNP groups, a change in morphology was observed, with more circular shapes and a decrease in size, as well as some reniform nuclei compared to the negative control group; in the positive control group (H<sub>2</sub>O<sub>2</sub>) a complete fragmentation of the nuclei was observed (Fig. 9C).

Oxidative stress can cause chromosomal damage, nuclear abnormalities, and cytogenetic alterations. Some researchers have reported that reniform nuclei have a cytological cause, while others consider that genotoxic effects may induce nuclear morphological changes. 55,56 Furthermore, excessive production of ROS within cellular mitochondria can potentially interfere

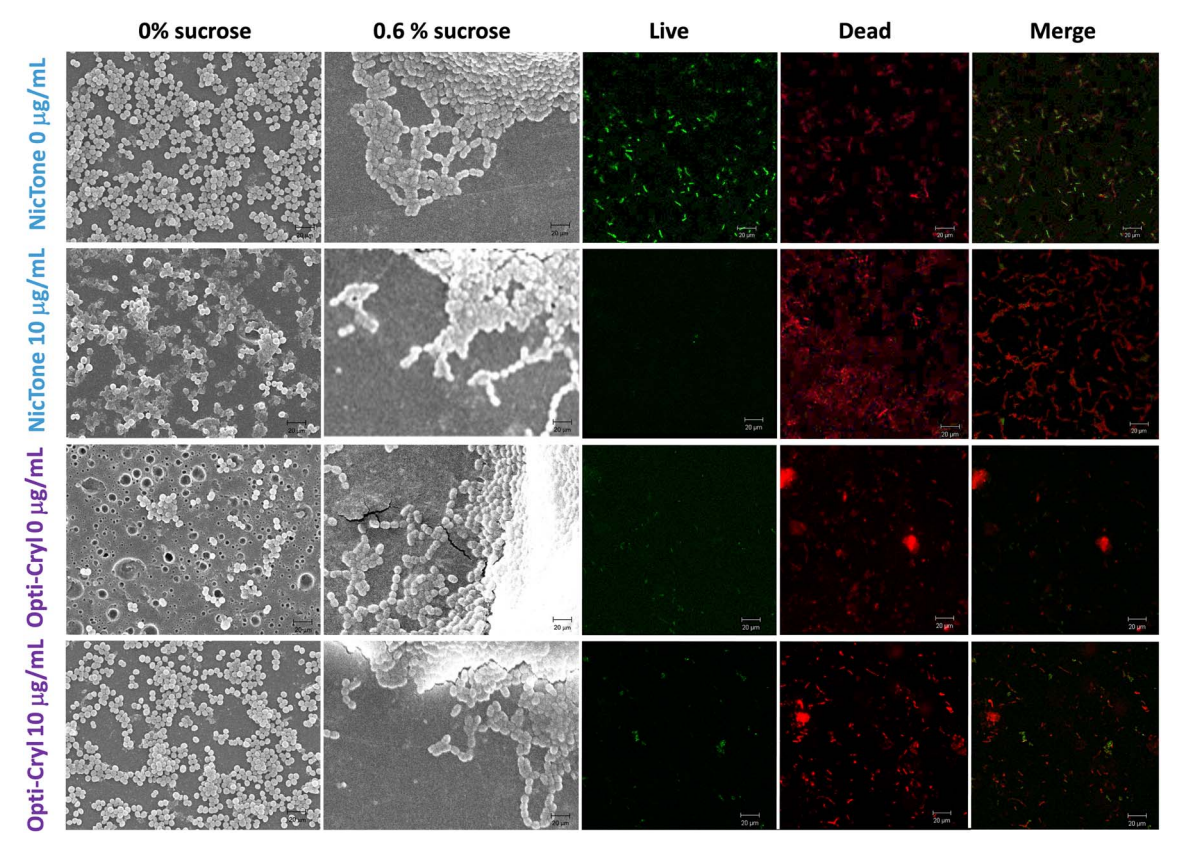


Fig. 8 Scanning electron microscopy and confocal fluorescence microscopy of S. mutans biofilms. Scanning electron microscopy at 6500× magnification shows the growth of the biofilm on the acrylic resin; a higher production of extracellular polysaccharides can be observed in the presence of 0.6% sucrose, which favors their formation; the incorporation of AgNPs allows the reduction of the density of the bacterial growth structure as observed in the NicTone group at 10 µg mL<sup>-1</sup>. Confocal microscopy images of biofilms stained with a Live/Dead™ BacLight bacterial viability kit show live cells in green and dead cells in red, indicating a greater presence of dead biofilms in the NicTone 10  $\mu$ g mL<sup>-1</sup> AgNPs group (magnification  $40\times$  and scale bar 20  $\mu$ m).

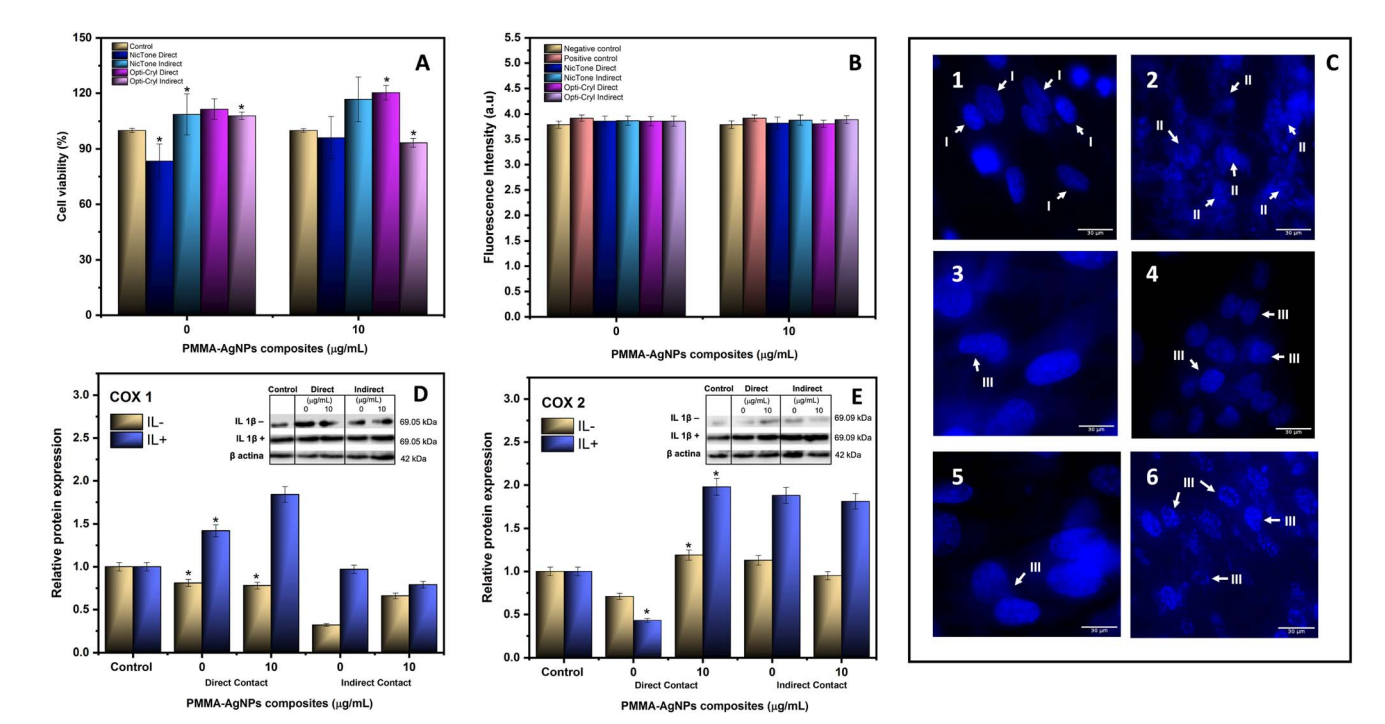


Fig. 9 Biological assays of PMMA and PMMA–AgNP composites in direct and indirect contact with HGF. Groups: Opti–Cryl and NicTone, AgNPs concentrations of 0 and 10 μg mL $^{-1}$ . (A) Cytotoxicity determined by MTT assay. Optical density 570 nm. Abs. range (0.211–1.857). Each value in the graph represents the percentage of the mean and S.D. One-way ANOVA was performed, followed by *post hoc* Tukey's test; (\*) represents concentrations with a significant difference p < 0.001, n = 9. (B) Oxidative stress induced by the intracellular ROS fluorometric assay. Negative control: sterile medium; positive control,  $H_2O_2$  2 mM. Optical density  $\lambda_{ex} = 490/\lambda_{em} = 520$  nm. Abs. range (3.788–3.814). Each value in the graph represents the mean and S.D. One-way ANOVA was performed for p > 0.05, and n = 9. (C) 63× micrograph of nuclear morphology by DAPI staining using fluorescence microscopy. (1) Negative control: HGF in the culture medium; (B) positive control ( $H_2O_2$  at 2 mM), (3) NicTone 0 μg mL; (4) NicTone 10 μg mL; (5) Opti–Cryl 0 μg mL; (6) Opti–Cryl 10 μg mL $^{-1}$ . The arrowheads indicate (I) normal morphology, (II) fragmented nuclei, (III) reniform nuclei, and (IV) shrunken nuclei (n = 3). (D) and (E) Western blotting showing the relative protein expression of anti–COX-1, anti–COX-2, and β-actin, and image analysis of western blot bands was performed by densitometry. Negative control: untreated cells (IL $^{-1}$ ); positive control: cells induced in a proinflammatory state (IL $^{+1}$ ) (n = 3).

with the proper mediation of cytochrome c release, which then triggers the activation of caspase-3, and consequently, can induce cell apoptosis.<sup>57</sup>

Tests for genotoxicity analysis are performed by different methods, such as the determination of DNA/protein cross-linking coefficients, mitochondrial enzymatic activity, cell proliferation, DNA break repair, mitotic index, comet assay, identification of damage, chromosomal aberrations and alterations in nuclear morphology. However, there are few studies reported in the literature to determine the genotoxicity of PMMA; Acosta-Torres *et al.* did not find alterations related to nuclear alterations when analyzing polymers with and without AgNPs, <sup>22</sup> while others researchers identified genotoxic effects after 24 h of exposure to MMA vapour. <sup>59</sup>

#### Proinflammatory response and residual monomers

The toxic and inflammatory processes of PMMA reported in articles relate this response to the polymerization effect resulting from the exothermic reaction of the methacrylates in the material and the resulting residual monomers; this release can induce genetic mutations, causing cell cycle delay and cell death.  $^{60}$  Campaner *et al.* and Bacali *et al.* identified the presence of TNF- $\alpha$  as an inflammatory cellular response in PMMA in

direct and indirect contact.<sup>60,61</sup> It was also found that the addition of 2% AgNPs to PMMA had an anti-inflammatory effect.<sup>61</sup> In relation to the release of pro-inflammatory cytokines in HGF, a significant release of cytokines has been reported in indirect contact with PMMA.<sup>61</sup> On the other hand, Trubiani *et al.* reported that after 24 h of contact with PMMA, the release of interleukin-6 (IL-6) and interleukin-8 (IL-8) was identified, with lower levels observed when the samples were polished, favoring a reduction in the gingival inflammatory process.<sup>62</sup>

To assess the inflammatory response in our study, HGFs were induced into a proinflammatory state with IL-1- $\beta$ , which among its many functions, induces the production of IL-6. Cyclooxygenases (COX) 1 and 2, which are key enzymes involved in the synthesis of prostaglandins (PG), were detected. The COX-1 isoform maintains a normal physiological production of prostaglandins, while COX-2 is produced by cytokines and endotoxins responsible for inflammatory processes.<sup>63</sup> Our results showed that PMMA with 10  $\mu$ g mL<sup>-1</sup> AgNPs both in direct and indirect contact did not show COX-1 related changes (Fig. 9D); however, in synergy with a pro-inflammatory state, an increase in COX-2 expression was identified in the case of direct contact with PMMA with 10  $\mu$ g mL<sup>-1</sup> AgNPs (p < 0.05) (Fig. 9E).

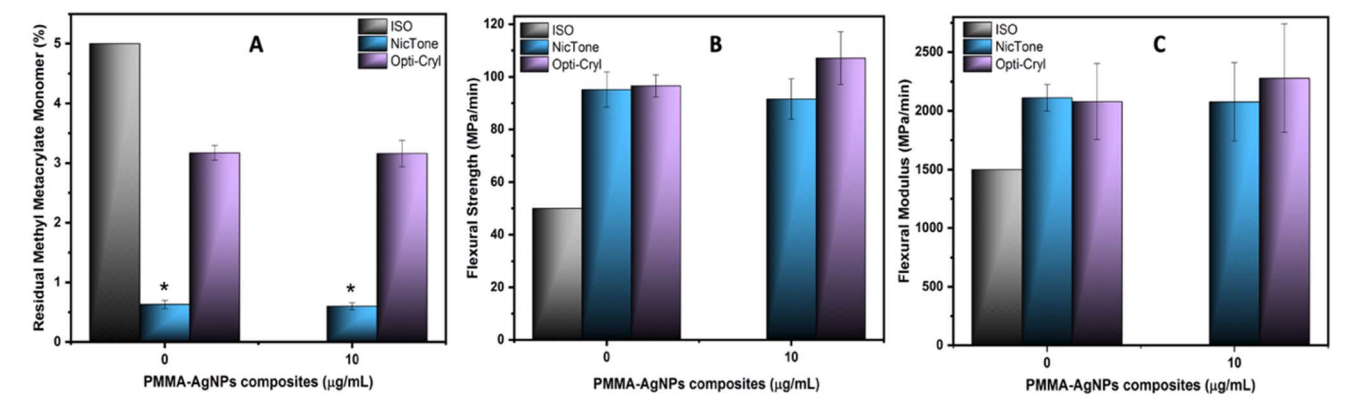


Fig. 10 (A) Residual monomers of Opti-Cryl and NicTone self-curing PMMA. AgNP concentrations of 0 and 10 g mL<sup>-1</sup>. Each value in the graph represents a percentage and S.D. One-way ANOVA was performed, along with post hoc Tukey; (\*) represents concentrations with significant differences (p < 0.001, n = 3). (B) Flexural strength in the 3-point test for the PMMA and PMMA-AgNP composites. Standard (ISO 20795-2 values, minimum 50 Mpa). Each value in the graph represents the mean and S.D. One-way analysis of variance (ANOVA) was performed. p > 0.05, n = 10. (C) Flexural moduli of PMMA and PMMA-AgNP composites. Standard (ISO 20795-2, minimum 1500 Mpa). Each value in the graph represents the mean and S.D. One-way ANOVA was performed. p > 0.05, n = 10.

In relation to the residual monomer in Fig. 10A, the release amount does not change in the two brands analyzed with and without AgNPs, considering that both commercial self-curing PMMA comply with the provisions of the ISO-20975-2 STAN-DARD,<sup>36</sup> in Section 5.2, because the maximum mass fraction of the residual monomer is less than 5.0%. In the specific case of Opti-Cryl, the standard deviation was large, although the addition of AgNPs did not change the system. This difference may be because the experimental group was not completely soluble in tetrahydrofuran (THF);<sup>37</sup> however the solvent swells the sample sufficiently to extract any possible residual monomer, which does not affect the analysis of the residual monomer. Another possible explanation is that the sample contains a mixture of acrylates or different monomers that cross-link more strongly.

#### Mechanical properties

In the results of the mechanical tests of strength and flexural modulus, values above the norm were observed for Opti-Cryl and NicTone with 0  $\mu g\ mL^{-1}$  (control groups; Fig. 10). In Opti-Cryl with 10 μg mL<sup>-1</sup> AgNPs, an increase was observed compared to its control group and in NicTone with 10 µg mL<sup>-1</sup> of AgNPs a slight decrease was observed, although no statistically significant differences were found (p > 0.05) (Fig. 10B and C).

Campos et al. reported a flexural strength of 67.89  $\pm$ 8.54 MPa for Opti-Cryl, which is above the ISO standard; when AgNPs were incorporated into the material, they reported improved mechanical properties (69.02 ± 6.14 MPa);<sup>45</sup> our results show higher values (from 90 MPa) in the two brands of PMMA studied, even before the incorporation of AgNPs.

Research has shown that the mixing method can affect the dispersion of nanoparticles in a matrix. Furthermore, the type of NPs incorporated, their size, shape and concentration can determine the interaction with the polymer matrix. 64,65 In our results, both mechanical tests for the NicTone group with 10 µg mL<sup>-1</sup> AgNPs showed a slight decrease in comparison with the

control group (0 µg mL<sup>-1</sup>). This can be explained by the dispersion of AgNPs in the polymer matrix, which reduced the reaction of the monomer and consequently the physical properties.65 However, these values were above the standard, so we can deduce that the proposed technique of adding AgNPs to the monomer avoids agglomeration sites that could negatively affect the physical properties of the nanocomposite.

It can be observed that the biological activity and mechanical characteristics of PMMA-AgNP composites are slightly affected, depending on the concentration and the incorporation technique of the AgNPs utilized. The cytotoxicity assays indicated that higher concentrations of AgNPs, up to 10  $\mu$ g mL<sup>-1</sup>, can be integrated into PMMA composites without affecting the cell viability (below 80%). This suggests that the developed biocomposite can retain non-cytotoxic behavior, even under conditions that cause slight cell viability loss. This compatibility can be explained by the encapsulation of the AgNPs that occurred during the polymerization process, diminishing the chances of inward-cell exposure to the particles, and therefore, toxic interactions with the cells are minimized.64

Interestingly, the same method of encapsulation may also be responsible for the mechanical properties observed. For instance, addition of 10 µg mL<sup>-1</sup> AgNPs resulted in a mild decrease in flexural strength in the NicTone group but an improvement in the Opti-Cryl group. These variations could be attributed to AgNP dispersions and interactions in the polymeric matrix.65 Inadequate dispersion can lead to microstructural inconsistencies, which reduces the monomer-polymer interaction and slightly compromises the mechanical properties, as observed in NicTone. In contrast, improved dispersion, as observed in Opti-Cryl, can enhance the reinforcing effect of AgNPs, leading to better mechanical performance. 64,65

The encapsulation of AgNPs also seems to provide a potential reduction in trade-off between cytotoxicity and mechanical integrity. High concentrations of AgNPs have been linked with cytotoxicity in aqueous environments,53 but a polymeric matrix such as PMMA can hinder their release and enable diffusion over time. Our results show that not only we can achieve cell viability, but we also maintain mechanical properties above ISO standards.

## Conclusions

A greater decrease in bacterial adhesion was observed with the incorporation of AgNPs into NicTone brand PMMA at 10 µg mL<sup>-1</sup>. At this concentration, cellular bioassays did not show cytotoxicity or ROS expression, but a genotoxicity response was observed with reniform nuclei, confirming that it is necessary to continue with more specific experiments to determine the mechanisms of inflammation or alteration in host cells. The present study demonstrates that the incorporation of AgNPs into PMMA matrices improves certain functional properties of the material, particularly its antimicrobial behaviour and mechanical performance; it was observed that the effect of AgNPs depends significantly on their concentration. This behaviour influences both the mechanical properties of the compound and its interaction with biological cells, highlighting the importance of optimizing the concentrations to avoid adverse effects such as cytotoxicity or embrittlement of the material. Overall, the cell bioassays analyzed in this research did not show any significant inflammatory effect with the PMMA-AgNP nanocomposite, suggesting that it could be a potential candidate for dental applications.

## Data availability

Raw data are available from the corresponding author on reasonable request.

## **Author contributions**

Conceptualization: C. A. L.-A., L. S. A.-T., and R. G.-C. Methodology and validation: L. S. A.-T., R. G.-C., and R. M. Result interpretation: C. A. L.-A., M. F., M. R.-G., M. J. A., and R. A. D.-P. HPLC analyses: M. F., M. R.-G., M. J. A. and S. C. Data curation: C. A. L.-A., M. F. R., G.-C. and R. M. Supervision: L. S. A.-T. Manuscript writing: C. A. L.-A. Manuscript review and editing: L. S. A.-T., R. G.-C., R. M., M. F., M. R.-G., M. J. A., R. A. D.-P. and S. C.

## Conflicts of interest

There are no conflicts of interest to declare.

# Acknowledgements

The authors acknowledge the financial support from UNAM-DGAPA-PAPIIT: IN211922, IT200922 & TA200123 and PAPIME: PE203622. They also acknowledge the technical assistance from Ing. Nydia Hernandez Rios (fluorescence microscopy), Ing. Ma. Lourdes Palma Tirado (TEM analysis), INB-Juriquilla, Mexico; Shigeru Amano (SEM images), Meikai University, Japan; M. C. Elizabeth Hernandez Alvarez for analytical support in the

determination of trace elements (ICP-MS), Instituto de Geofisíca, UNAM, Mexico and Dr Dulce Guzman Rocha (XRD pattern), Centro de Investigaciones en Óptica, León, Guanajuato, Mexico.

## References

- A. M. Díez-Pascual, Int. J. Mol. Sci., 2022, 23, 10288, DOI: 10.3390/ijms231810288.
- 2 H. Kaur and A. Thakur, *Mater. Today: Proc.*, 2022, **50**, 1619–1625, DOI: **10.1016/j.matpr.2021.09.125**.
- 3 R. de Souza Leão, S. L. D. de Moraes, J. M. de Luna Gomes, C. A. A. Lemos, B. G. da Silva Casado, B. C. do Egito Vasconcelos and E. P. Pellizzer, *Mater. Sci. Eng.*, 2020, **106**, 110292, DOI: **10.1016/j.msec.2019.110292**.
- 4 M. S. Zafar, M. S. Polymers, 2020, **12**, 10–2299. DOI: **10.3390/ polym12102299**.
- 5 S. M. Pituru, M. Greabu, A. Totan, M. Imre, M. Pantea, T. Spinu, A. M. C. Tancu, N. O. Popoviciu, I. Stanescu and E. Ionescu, *Materials*, 2020, 13, 2894, DOI: 10.3390/ ma13132894.
- 6 K. Chęcińska, M. Chęciński, M. Sikora, Z. Nowak, S. Karwan and D. Chlubek, *Polymers*, 2022, 14, 1047, DOI: 10.3390/polym14051047.
- 7 I. Domagała, L. Gil, M. Firlej, D. Pieniak, J. Selech, D. Romek and B. Biedziak, *Adv. Sci. Technol.*, 2020, 14, 4, DOI: 10.12913/ 22998624/127437.
- 8 G. Lombardo, F. Vena, P. Negri, S. Pagano, C. Barilotti, L. Paglia, S. Colombo, M. Orso and S. Cianetti, *Eur. J. Paediatr. Dent.*, 2020, 21(2), 115–122, DOI: 10.23804/ejpd.2020.21.02.05.
- M. S. Alhammadi, E. Halboub, M. S. Fayed, A. Labib and C. El-Saaidi, *Dent. Press J. Orthod.*, 2018, 23(6), 40, DOI: 10.1590/2177-6709.23.6.40.e1-10.onl.
- 10 J. Murrieta-Pruneda, D. Varela-Ramírez, A. Rojano-Santillán, M. Adriano-Anaya and T. Caudillo-Joya, *J. Oral. Res.*, 2020, 9(4), 293–299, DOI: 10.17126/joralres.2020.070.
- 11 J. O. Jorge, L. Corradi-Dias, C. Flores-Mir, I. A. Pordeus, S. M. Paiva and L. G. Abreu. The journal of evidence-based dental practice, 2020, 20, 3, 101423. doi: DOI: 10.1016/ j.jebdp.2020.101423.
- 12 J. Bächle, C. Merle, S. Hahnel and M. Rosentritt, *Materials*, 2023, **16**(6), 2373, DOI: **10.3390/ma16062373**.
- 13 X. Wei, L. Gao, K. Wu, Y. Pan, L. Jiang, H. Lin and H. Cheng, *Clin. Oral Investig.*, 2022, **26**(12), 7287–7297, DOI: **10.1007**/**s00784-022-04689-2**.
- 14 S. Keleştemur, Z. Çobandede and M. Çulha, *Colloids Surf., B*, 2020, **188**, 110765, DOI: **10.1016/j.colsurfb.2019.110765**.
- A. Delgado, J. Carvalho, G. Borrecho, T. Nascimento,
   M. E. Silva, S. A. Félix and J. J. Mendes, *Contemp. Clin. Dent.*, 2018, 9(3), 400–405, DOI: 10.4103/ccd.ccd\_141\_18.
- 16 T. Vanishree, G. S. Panchmal, R. Shenoy, P. Jodalli, L. Sonde and N. Kundapur, *Oral Health Prev. Dent.*, 2017, **15**(5), 453–459, DOI: **10**.3290/j.ohpd.a38776.
- 17 C. Shukla, R. K. Maurya, V. Singh and M. Tijare, *Dent. Res. J.*, 2016, **13**(4), 309–314, DOI: **10.4103**/1735-3327.187876.

- 18 N. Farhadian, R. Usefi Mashoof, S. Khanizadeh, E. Ghaderi, M. Farhadian and A. Miresmaeili, Am. J. Orthod. Dentofacial Orthop., 2016, **149**(2), 155-160, DOI: j.ajodo.2015.07.031.
- 19 E. Chimenos-Küstner, M. L. Giovannoni and M. Schemel-Suárez, Med. Clínica, 2017, 149(7), 305-309, DOI: 10.1016/ j.medcli.2017.05.0.
- 20 M. A. Hug, Int. J. Mol. Sci., 2020, 21(4), 1510, DOI: 10.3390/ ijms21041510.
- 21 J. C. Flores-Arriaga, R. Garcia-Contreras, G. Villanueva-Sanchez and L. S. Acosta-Torres, Appl. Sci., 2020, 10(11), 4007, DOI: 10.3390/app10114007.
- 22 L. S. Acosta-Torres, I. Mendieta, R. E. Nuñez-Anita, M. Cajero-Juárez and V. M. Castaño, Int. J. Nanomed., 2012, 7, 4777-4786, DOI: 10.2147/IJN.S32391.
- 23 S. P. Singh, S. K. Sharma and D. Y. Kim, Solid State Sci., 2020, 99, 106046, DOI: 10.1016/j.solidstatesciences.2019.106046.
- 24 F. Yousefi, S. B. Mousavi, S. Z. Heris and S. Naghash-Hamed, Sci. Rep., 2023, 13(1), 7116, DOI: 10.1038/s41598-023-34120-
- 25 M. Cascione, V. De Matteis, P. Pellegrino, G. Albanese, M. L. De Giorgi, F. Paladini and R. Rinaldi, Nanomaterials, 2021, 11(8), 2027, DOI: 10.3390/nano11082027.
- 26 A. M. Alsaad, A. A. Ahmad, A. R. Al Dairy, A. S. Al-anbar and Q. M. Al-Bataineh, Results Phys., 2020, 19, 103463, DOI: 10.1016/j.rinp.2020.103463.
- 27 A. Nabhan, M. Taha and N. M. Ghazaly, Polym. Test., 2023, 117, 107848, DOI: 10.1016/j.polymertesting.2022.107848.
- 28 R. Bahrami, F. Gharibpour, M. Pourhajibagher and A. Bahador, Int. Orthod., 2024, 22(2), 100846, DOI: 10.1016/ j.ortho.2024.100846.
- 29 H. A Widatalla, L. F. Yassin, A. A. Alrasheid, S. A. R. Ahmed, M. O. Widdatallah, S. H. Eltilib and A. A. Mohamed, Nanoscale Adv., 2022, 4(3), 911-915, DOI: 10.1039/ d1na00509j.
- 30 C. Takahashi and K. Moriguchi, Nanoscale Adv., 2024, 6(20), 5020-5030, DOI: 10.1039/d4na00249k.
- 31 M. C. R. Pinheiro, J. A. O. Carneiro, M. M. Pithon and E. F. Martinez, Mater. Res., 2021, 24(2), e20200115, DOI: 10.1590/1980-5373-MR-2020-0115.
- 32 C. A. Lopez-Ayuso, R. Garcia-Contreras, R. Manisekaran, M. Figueroa, M. C. Arenas-Arrocena, G. Hernandez-Padron and L. S. Acosta-Torres, RSC Adv., 2023, 13(42), 29784-29800, DOI: 10.1039/d3ra00201b.
- 33 Z. Pang, G. Zhou, J. Ewald, L. Chang, O. Hacariz, N. Basu and J. Xia, Nat. Protoc., 2023, 17(8), 1735-1761, DOI: 10.1038/ s41596-022-00710-w.
- 34 E. Grela, J. Kozłowska and A. Grabowiecka, Acta Histochem., 2018, **120**(4), 303–311, DOI: **10.1016/j.acthis.2018.03.007**.
- 35 E. Brambilla, A. Ionescu, G. Cazzaniga, V. Edefonti and M. Gagliani, Am. J. Dent., 2014, 27(3), 160-166.
- 36 International Organization for Standardization. 20795-2:2013, Dentistry-Base Polymers, Part 2: Orthodontic Base Polymers.
- 37 F. Solórzano Lemus, R. D. Venegas Lancón, V. Moreno Maldonado and S. López Morales, Rev. Odontol. Mex., 2010, 14(2), 91-98.

- 38 P. Serrano-Díaz, D. W. Williams, J. Vega-Arreguin, R. Manisekaran, J. Twigg, D. Morse and L. S. Acosta-Torres, Green Process. Synth., 2023, 12(1), 20228105, DOI: 10.1515/gps-2022-8105.
- 39 M. Marchioni, G. Veronesi, I. Worms, W. L. Ling, T. Gallon, D. Leonard and A. Deniaud, Nanoscale Horiz., 2020, 5(3), 507-513, DOI: 10.1039/c9nh00286c.
- 40 R. D. Rivera-Rangel, M. P. González-Muñoz, M. Avila-Rodriguez, T. A. Razo-Lazcano and C. Solans, Colloids 536, 60-67, DOI: Surf., 2018, 10.1016/ j.colsurfa.2017.07.051.
- 41 M. Mohammadlou, H. Jafarizadeh-Malmiri and H. Maghsoudi, Green Process. Synth., 2017, 6, 31-42, DOI: 10.1515/gps-2016-0075.
- 42 S. Jeong, S. Yang, Y. J. Lee and S. H. Lee, J. Mater. Chem. A, 2023, 11(25), 13409-13418, DOI: 10.1039/D3TA00691C.
- 43 M. D. Ferreira, L. C. D. S. Neta, G. C. Brandão and W. N. L. Dos Santos, Biotechnol. Appl. Biochem., 2023, 70(3), 1001-1014, DOI: 10.1002/bab.2415.
- 44 A. Kaddouri, B. Serier, K. Kaddouri, M. Belhouari and M. Frattura, Integrità Strutturale, 2020, 14, 53, pp. 66-80. doi: DOI: 10.3221/IGF-ESIS.53.06.
- 45 V. Campos, I. DeAlba-Montero, F. Ruiz, C. Butrón-Téllez Girón, E. García-García and M. Loredo-Tovías, Superficies Vacio, 2017, 30(4), 51-55, DOI: 10.47566/2017\_syv30\_1-040051.
- 46 Z. Tavaf, M. Tabatabaei, A. Khalafi-Nezhad and F. Panahi, Eur. J. Integr. Med., 2017, 12, 163-171, DOI: 10.1016/ j.eujim.2017.05.011.
- 47 X. Ma, J. Lang, P. Chen and R. Yang, AIChE J., 2021, 67, 12, DOI: 10.1002/aic.17468.
- 48 J. Méndez-Serrano, U. Velazquez-Enriquez, R. Contreras-Bulnes, I. De La Rosa-Gómez, T. Sawada R. Yamaguchi, Interciencia, 2020, 45(1), 23-27.
- 49 A. Chan, K. Ellepola, T. Truong, P. Balan, H. Koo and C. J. Seneviratne, Arch. Oral Biol., 2020, 119, 104886, DOI: 10.1016/j.archoralbio.2020.104886.
- 50 J. N. Cai, H. M. Choi and J. G. Jeon, J. Oral Microbiol., 2021, 13(1), 1910443, DOI: 10.1080/20002297.2021.1910443.
- 51 International Organization for Standardization, 10993-5, Part 5: t-est for in vitro cytotoxicity.
- 52 J. Sun, L. Wang, J. Wang, Y. Li, X. Zhou, X. Guo, T. Zhang and H. Guo, Dent. Mater. J., 2021, 40(5), 1100-1108, DOI: 10.4012/ dmj.2020-129.
- 53 M. C. R. Pinheiro, J. A. O. Carneiro, M. M. Pithon and E. F. Martinez, Mater. Res., 2021, 24, e20200115, DOI: 10.1590/1980-5373-MR-2020-0115.
- 54 A. Shenava, *Nanosci. Nanotechnol.-Asia*, 2023, **13**(3), 34-41, DOI: 10.2174/2210681213666230413090403.
- 55 I. Brandts, C. Barría, M. A. Martins, L. Franco-Martínez, A. Barreto, A. Tvarijonaviciute and M. Teles, J. Hazard. 2021, 403, 123590, DOI: 10.1016/ Mater., j.jhazmat.2020.123590.
- 56 A. Barreto, A. Dias, B. Duarte, E. Pinto, A. Almeida, T. Trindade and M. Oliveira, Sci. Total Environ., 2020, 716, 137026, DOI: 10.1016/j.scitotenv.2020.137026.

57 A. F. Khafaga, M. A. Naiel, M. A. Dawood and H. M. Abdel-Latif, *Aquat. Toxicol.*, 2020, 228, 105624, DOI: 10.1016/ j.aquatox.2020.105624.

Nanoscale Advances

- 58 R. Landsiedel, N. Honarvar, S. B. Seiffert, B. Oesch and F. Oesch, *Wiley Interdiscip. Rev.:Nanomed. Nanobiotechnol.*, 2022, 14(6), e1833, DOI: 10.1002/wnan.1833.
- 59 M. C. Arenas-Arrocena, L. Argueta-Figueroa, R. García-Contreras, O. Martínez-Arenas, B. Camacho-Flores, M. P. Rodriguez-Torres and L. S. Acosta-Torres, *Acrylic Polym. Healthcare*, 2017, 10, 43–74, DOI: 10.5772/intechopen.69066.
- 60 M. Campaner, A. S. Takamiya, S. B. Bitencourt, L. C. Mazza, S. H. P. de Oliveira, R. Shibayama and A. Pesqueira, *Arch. Oral Biol.*, 2020, 111, 104643, DOI: 10.1016/j.archoralbio.2019.104643.

- 61 C. Bacali, I. Baldea, M. Moldovan, R. Carpa, D. E. Olteanu, G. A. Filip and F. Badea, *Clin. Oral Invest.*, 2020, 24, 2713– 2725, DOI: 10.1007/s00784-019-03133-2.
- 62 O. Trubiani, E. Toniato, D. Di Iorio, F. Diomede, I. Merciaro,
   C. D'Arcangelo and T. Oriana, *Int. J. Immunopathol. Pharmacol.*, 2012, 25(3), 637–643, DOI: 10.1177/039463201202500310.
- 63 M. M. Taskan and F. Gevrek, Niger. J. Clin. Pract., 2020, 23(1), 46-53, DOI: 10.4103/njcp.njcp\_349\_19.
- 64 P. Soleymanijadidi, M. Moradi, F. Hamedirad, Z. Ghanavati, S. Maleki Dizaj and S. Salatin, *Bioengineering*, 2023, **10**(5), 559, DOI: **10.3390/bioengineering10050559**.
- 65 A. Mithran, J. Rakhra, S. K. Jain, M. Chikkanna, S. Gowrish, S. G. Pillai and A. S. Nayyar, *J. Orthod. Sci.*, 2023, 12(1), 64, DOI: 10.4103/jos.jos\_43\_23.